Electronic Supplementary Material

Patterning of carbon nanotube film for effective microwave absorption over 2–18 GHz

Xin Ran Cheng[1], Zu Jia Hu[1], Yi Fan Feng[1], Hui Li Yang[1], Shu Quan Gong[1], Jian Feng Zheng[2], and Jian Nong Wang (✉)[2]

1 School of Materials Science and Engineering, East China University of Science and Technology, 130 Meilong Road, Shanghai 200237, China
2 School of Mechanical and Power Engineering, East China University of Science and Technology, 130 Meilong Road, Shanghai 200237, China

E-mail: jnwang@ecust.edu.cn

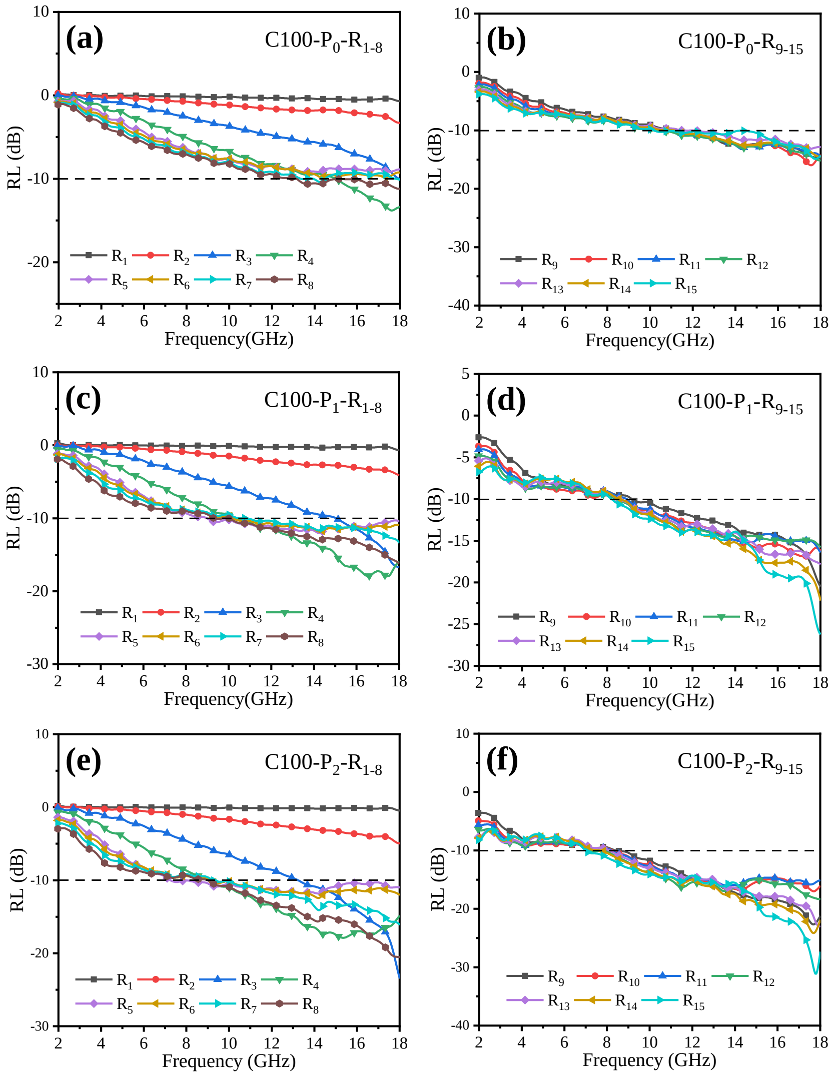

Fig. S1 Complete reflection-loss (RL) curves of the C100-based multilayer absorbers with PET interlayer numbers of P_0–P_2 over 2–18 GHz: **(a)(b)** C100-P_0; **(c)(d)** C100-P_1; and **(e)(f)** C100-P_2. The left and right panels show R_1–R_8 and R_9–R_{15}, respectively.

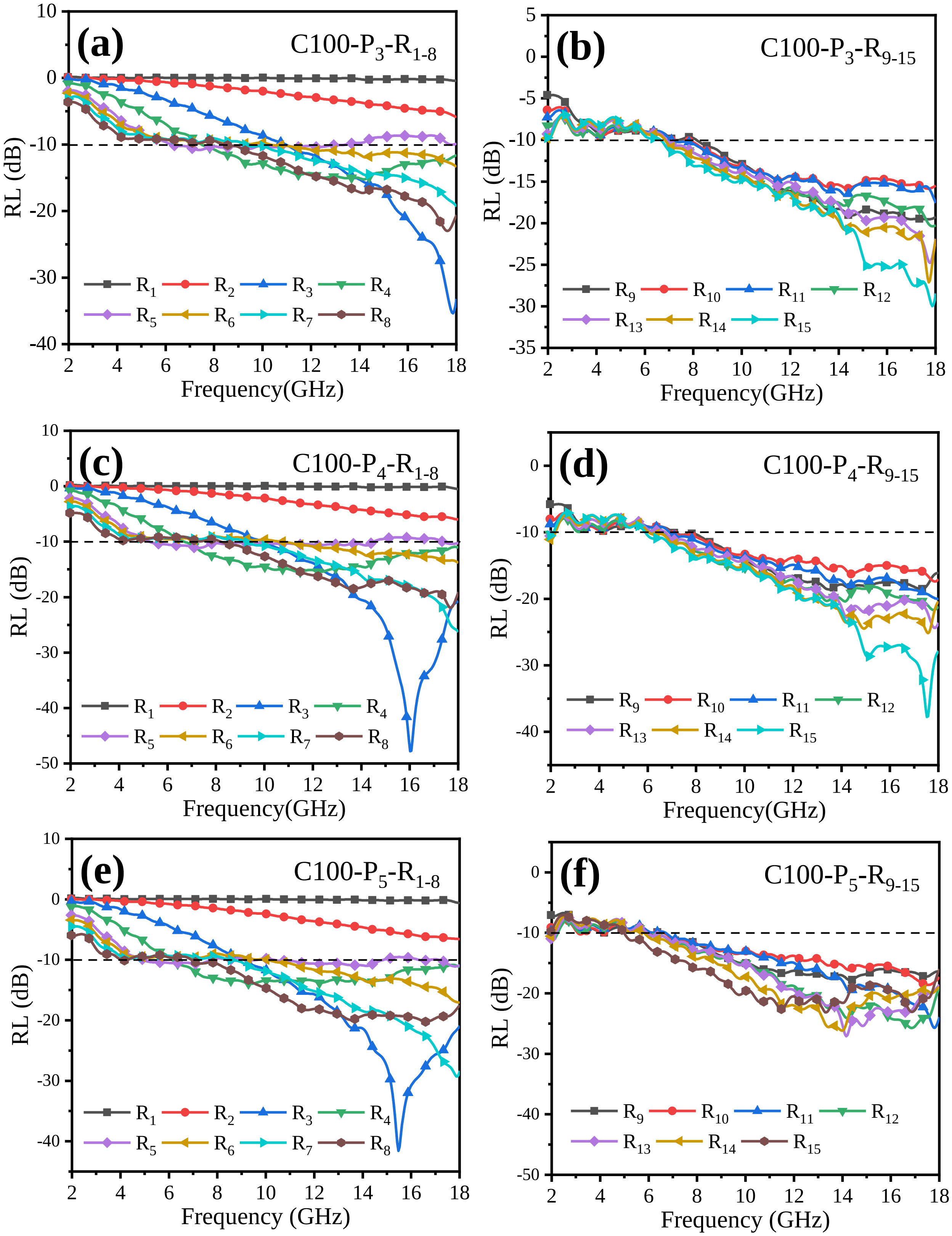

Fig. S2 Complete reflection-loss (RL) curves of the C100-based multilayer absorbers with PET interlayer numbers of P_3–P_5 over 2–18 GHz: **(a)(b)** C100-P_3; **(c)(d)** C100-P_4; and **(e)(f)** C100-P_5. The left and right panels show R_1–R_8 and R_9–R_{15}, respectively.

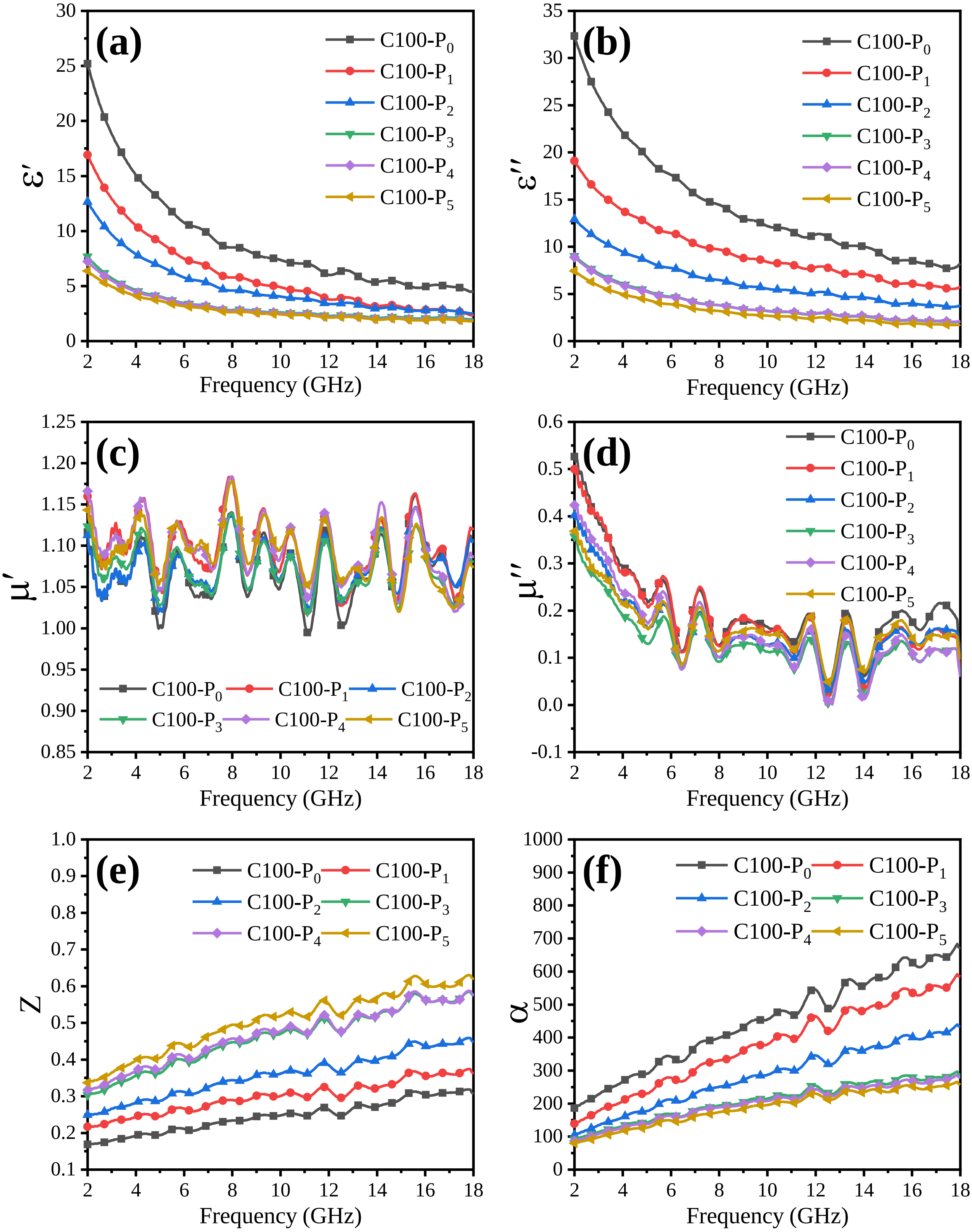

Fig. S3 Electromagnetic parameters and derived characteristics of representative C100/PET composite units containing one C100 functional sheet and zero to five PET interlayers over 2–18 GHz: **(a)** real and **(b)** imaginary parts of the complex relative permittivity; **(c)** real and **(d)** imaginary parts of the complex relative permeability; **(e)** normalized intrinsic impedance ratio, Z; and **(f)** attenuation constant, α. The permittivity and permeability were directly measured by the coaxial-line method, whereas Z and α were calculated from the measured electromagnetic parameters.

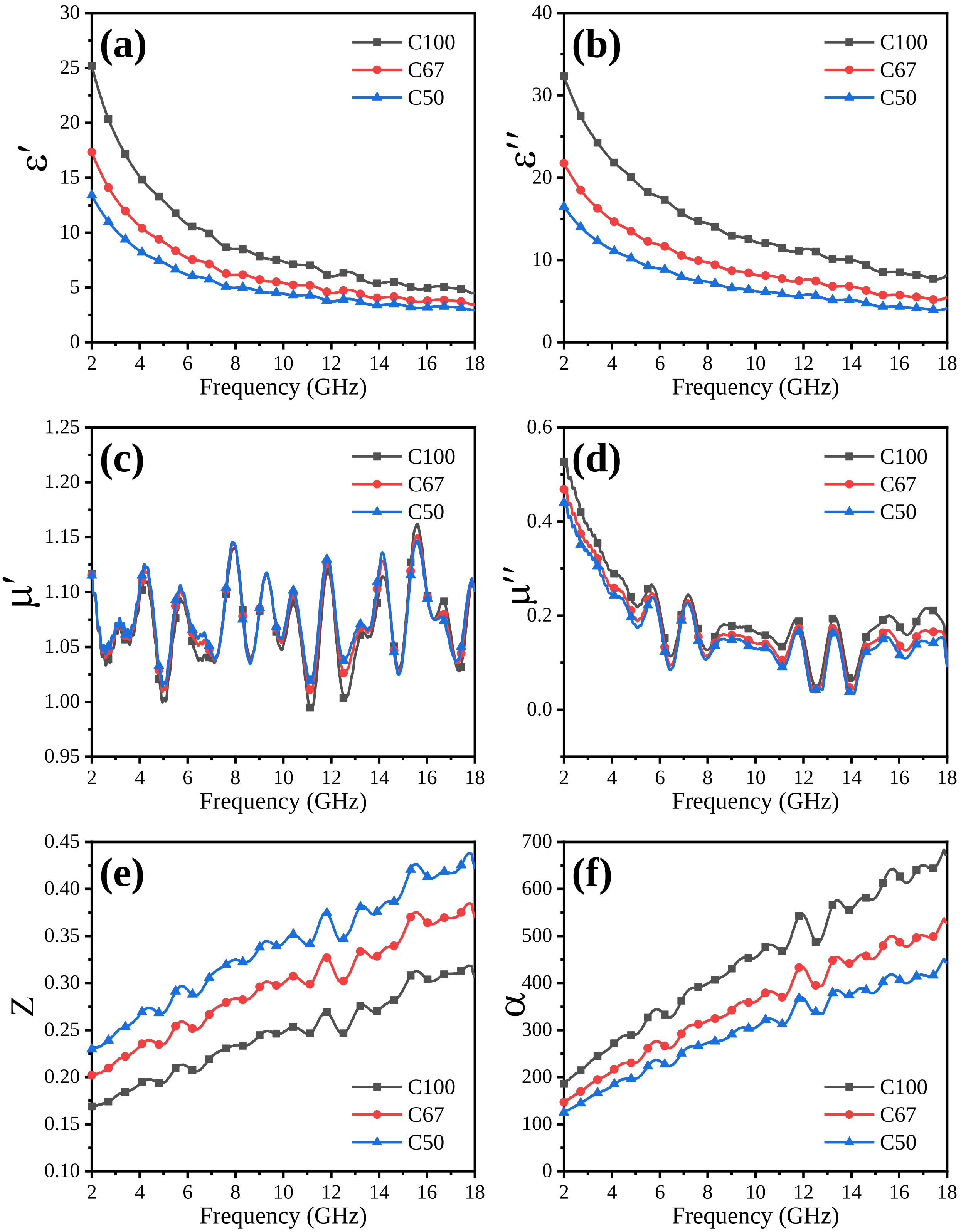

Fig. S4 Area-weighted equivalent electromagnetic parameters and derived characteristics of C100, C67, and C50 over 2–18 GHz: **(a)** real and **(b)** imaginary parts of the complex relative permittivity; **(c)** real and **(d)** imaginary parts of the complex relative permeability; **(e)** normalized intrinsic impedance ratio, *Z*; **(f)** attenuation constant, *α*. The parameters of C67 and C50 were estimated from the directly measured parameters of C100 and PET using the retained CNT-covered area fractions.

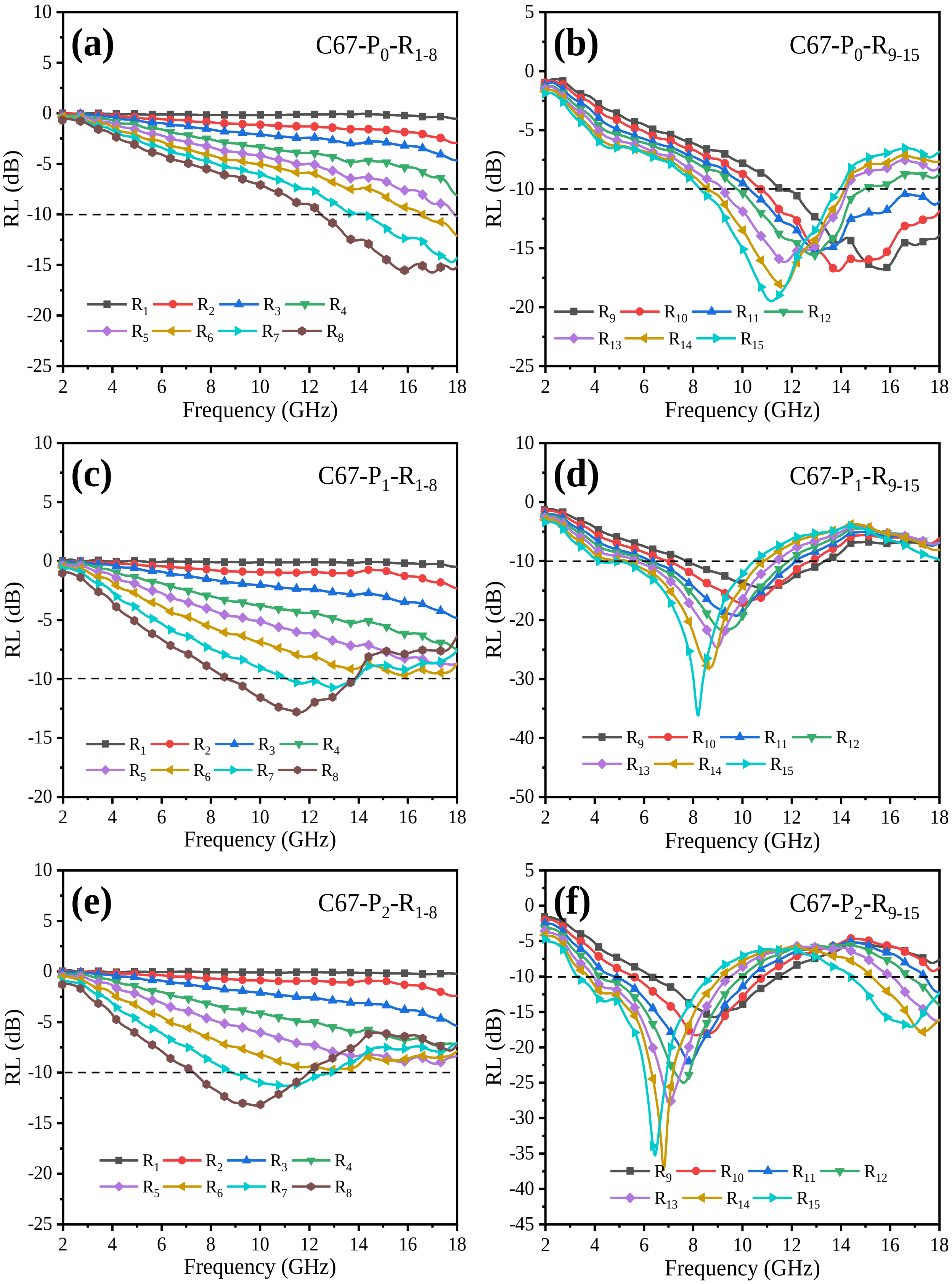

Fig. S5 Complete reflection-loss curves of the C67-based multilayer absorbers with PET interlayer numbers of P_0–P_2 over 2–18 GHz: **(a)(b)** C67-P_0; **(c)(d)** C67-P_1; and **(e)(f)** C67-P_2. The left and right panels show R_1–R_8 and R_9–R_{15}, respectively.

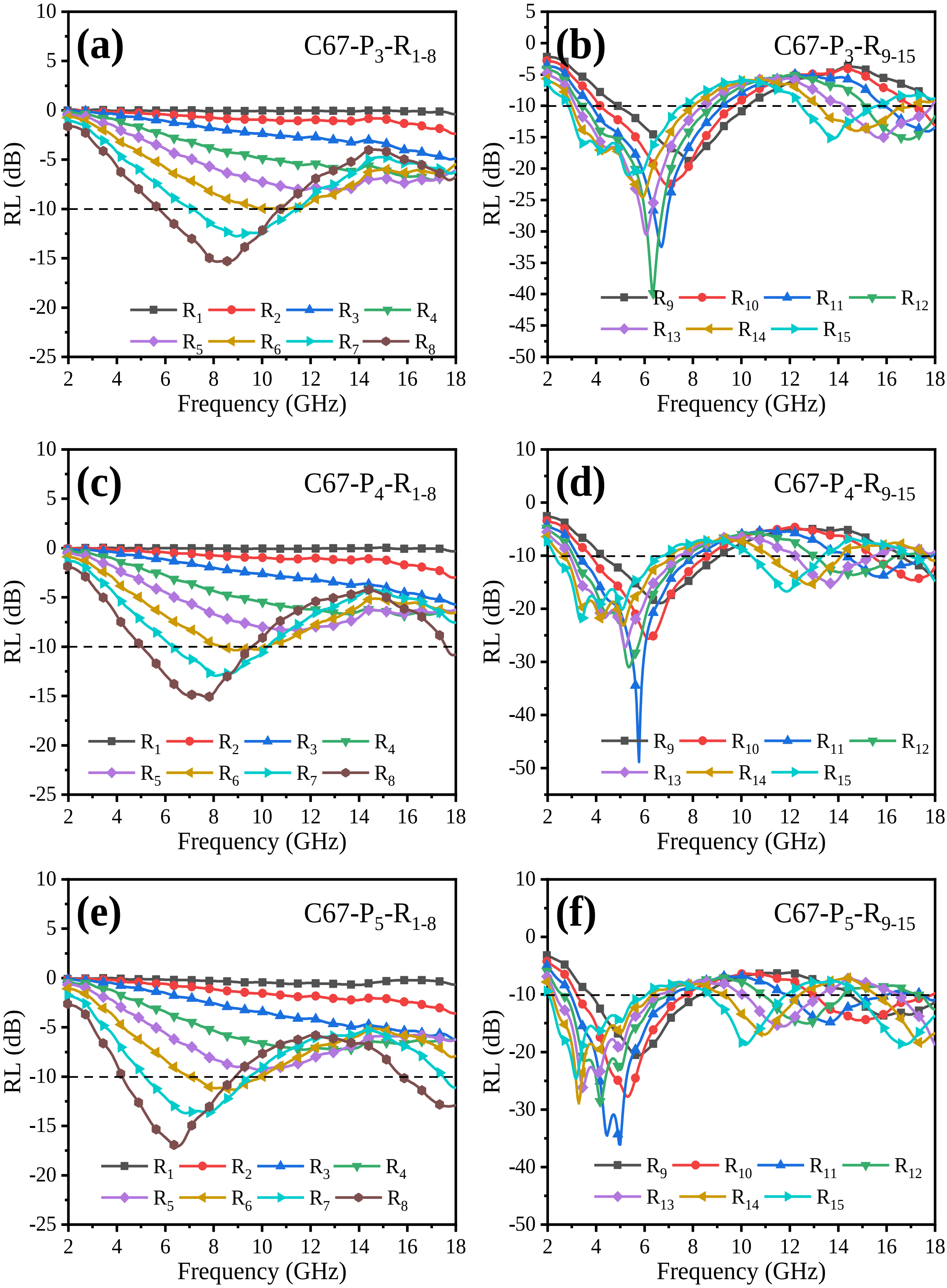

Fig. S6 Complete reflection-loss curves of the C67-based multilayer absorbers with PET interlayer numbers of P_3–P_5 over 2–18 GHz: **(a)(b)** C67-P_3; **(c)(d)** C67-P_4; **(e)(f)** C67-P_5. The left and right panels show R_1–R_8 and R_9–R_{15}, respectively.

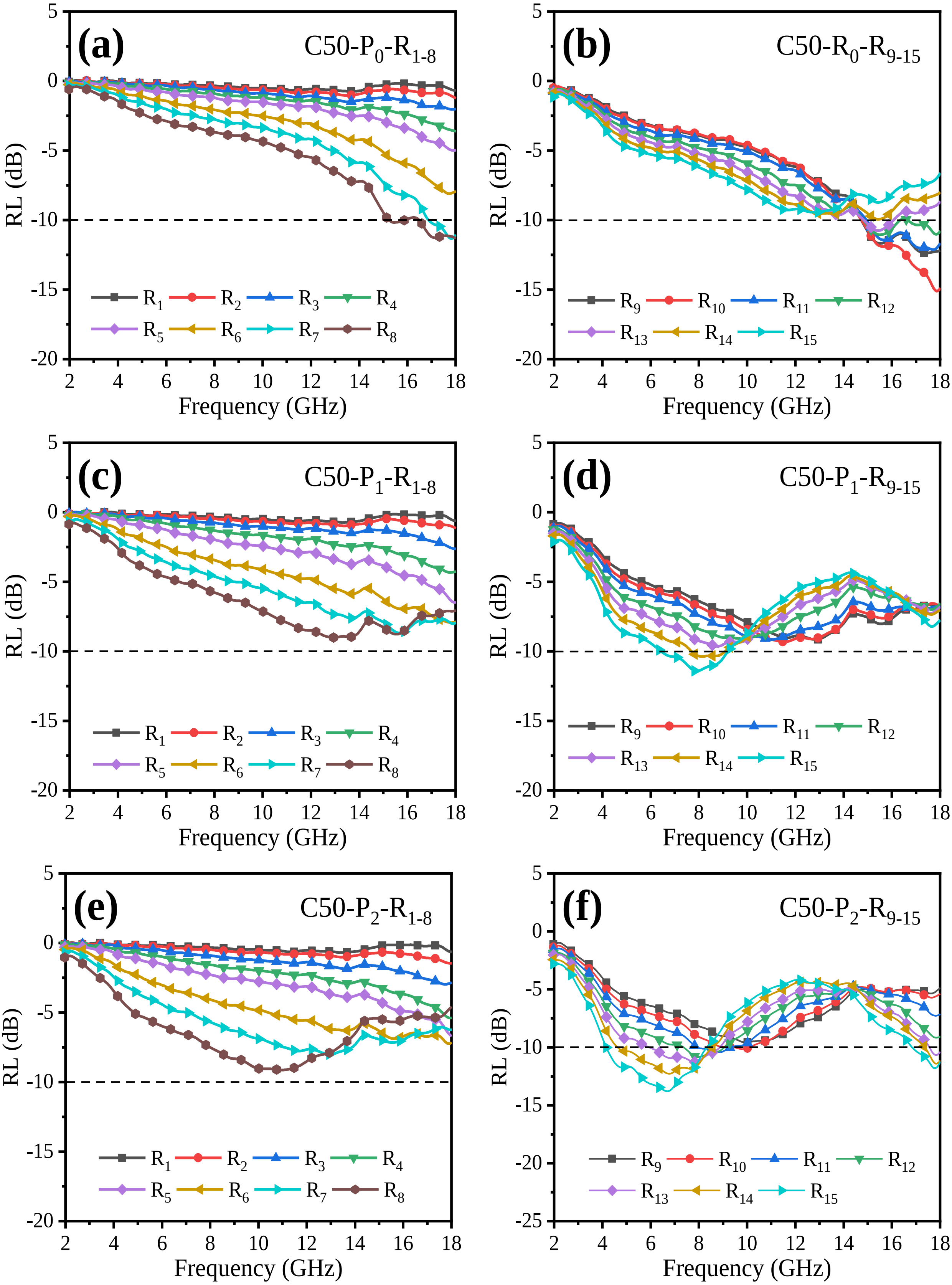

Fig. S7 Complete reflection-loss curves of the C50-based multilayer absorbers with PET interlayer numbers of P_0–P_2 over 2–18 GHz: **(a)(b)** C50-P_0; **(c)(d)** C50-P_1; and **(e)(f)** C50-P_2. The left and right panels show R_1–R_8 and R_9–R_{15}, respectively.

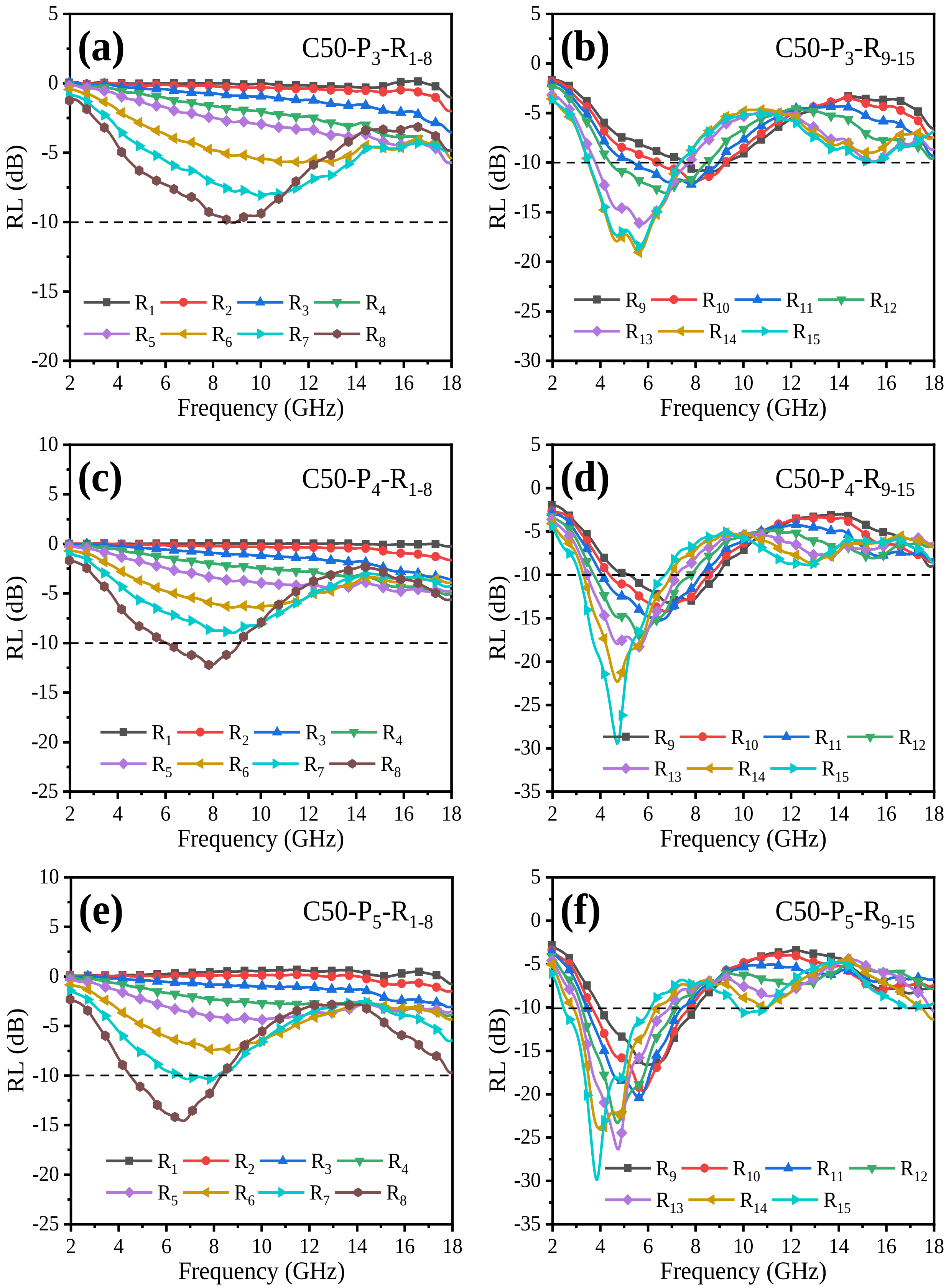

Fig. S8 Complete reflection-loss curves of the C50-based multilayer absorbers with PET interlayer numbers of P_3–P_5 over 2–18 GHz: **(a)(b)** C50-P_3; **(c)(d)** C50-P_4; and **(e)(f)** C50-P_5. The left and right panels show R_1–R_8 and R_9–R_{15}, respectively.

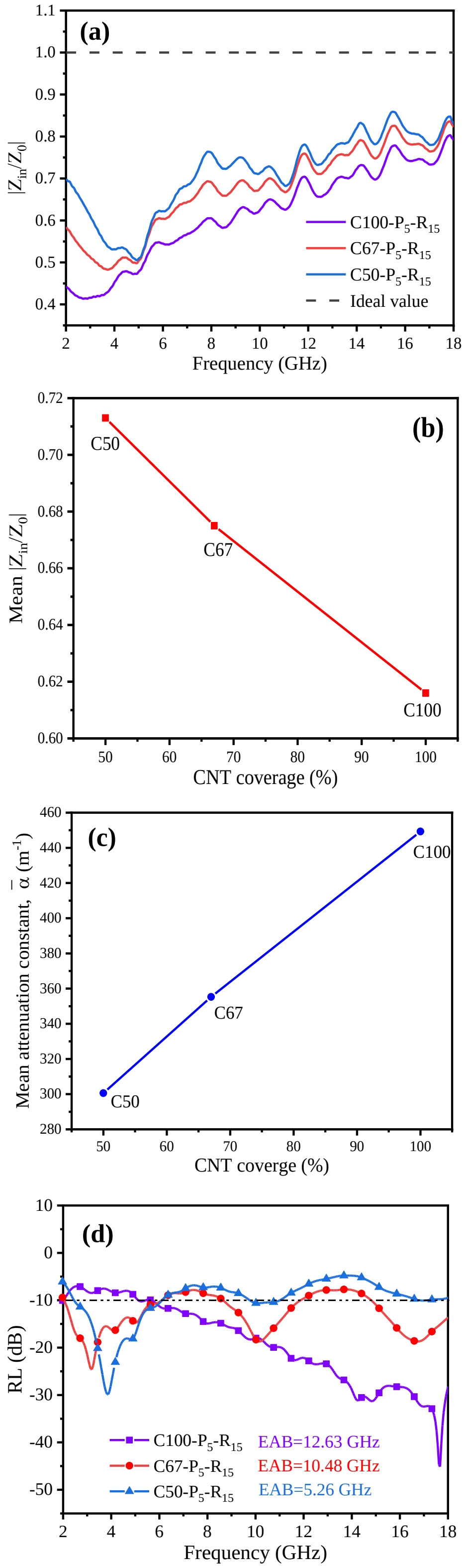

Fig. S9 Quantitative correlation between CNT coverage and the impedance–attenuation characteristics under the identical P_5-R_{15} configuration: **(a)** Calculated normalized input impedance magnitudes, $|Z_{in}/Z_0|$, of C100-P_5-R_{15}, C67-P_5-R_{15}, and C50-P_5-R_{15} based on the recursive multilayer transmission-line model (the horizontal dashed line represents the ideal impedance-matching condition of $|Z_{in}/Z_0| = 1$); **(b)** Frequency-averaged normalized input impedance magnitude as a function of CNT coverage; **(c)** Frequency-averaged attenuation constant of the equivalent C100, C67, and C50 functional sheets as a function of CNT coverage; **(d)** Measured RL curves of the three P_5-R_{15} structures.

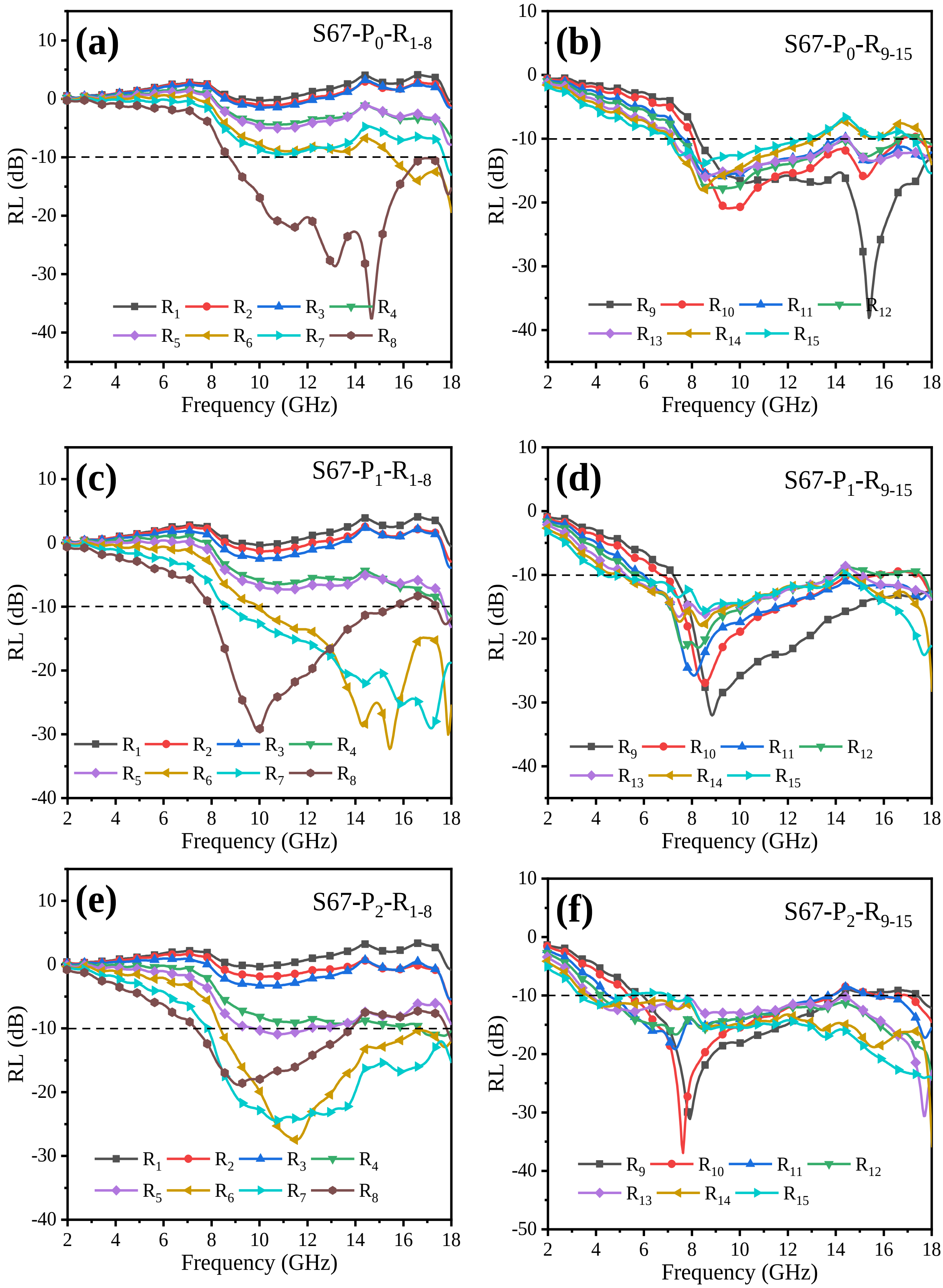

Fig. S10 Complete reflection-loss curves of the staggered S67-based multilayer absorbers with PET interlayer numbers of P_0–P_2 over 2–18 GHz: **(a)(b)** S67-P_0; **(c)(d)** S67-P_1; and **(e)(f)** S67-P_2. The left and right panels show R_1–R_8 and R_9–R_{15}, respectively.

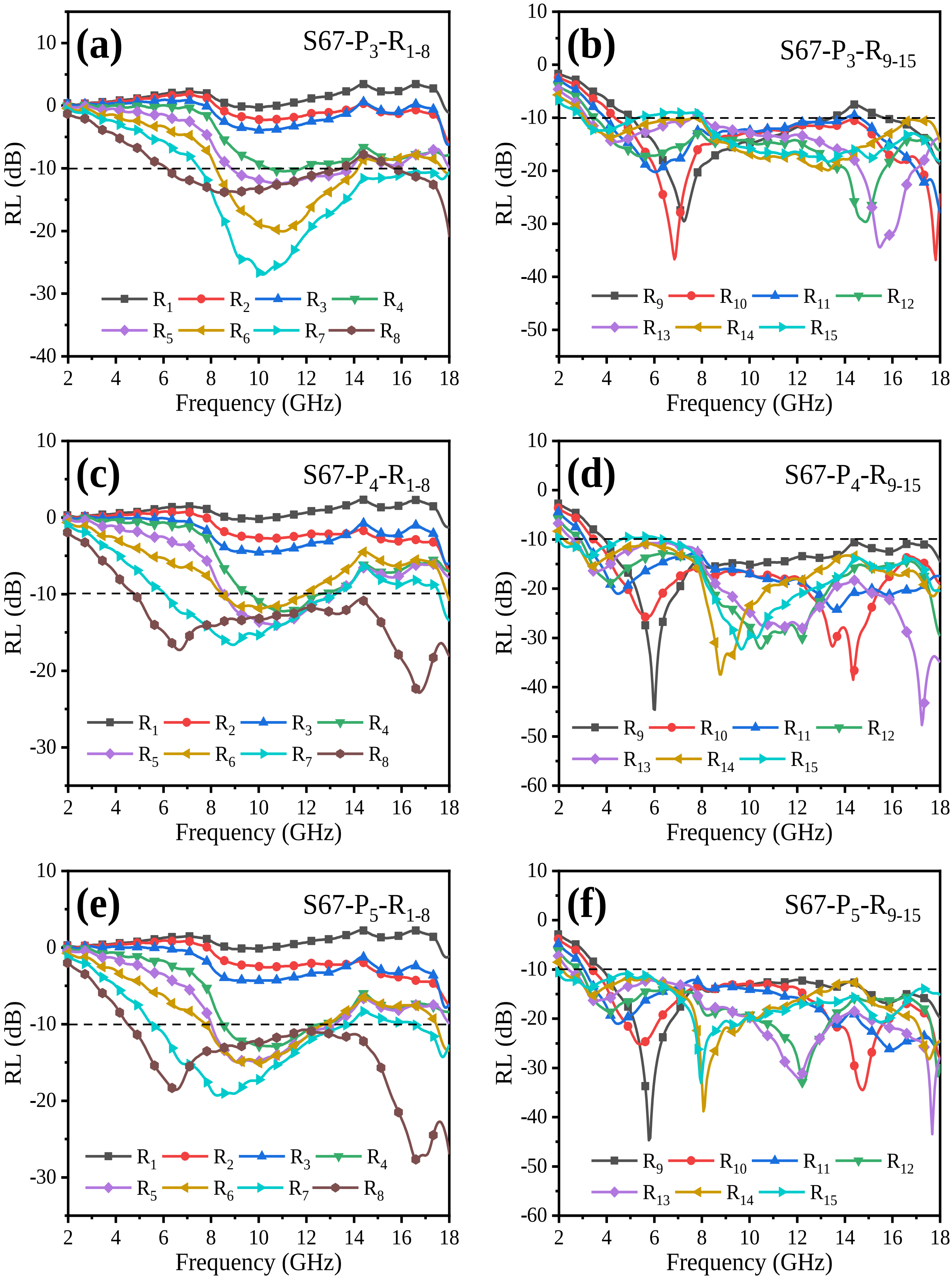

Fig. S11 Complete reflection-loss curves of the staggered S67-based multilayer absorbers with PET interlayer numbers of P_3–P_5 over 2–18 GHz: **(a)(b)** S67-P_3; **(c)(d)** S67-P_4; and **(e)(f)** S67-P_5. The left and right panels show R_1–R_8 and R_9–R_{15}, respectively.

Note S1: Multilayer transmission-line analysis

To quantitatively evaluate the influence of CNT coverage on the overall input-impedance characteristics of the multilayer absorbers, a recursive multilayer transmission-line model was established. The measured complex electromagnetic parameters of the C100 functional sheet and PET interlayer, together with the area-weighted equivalent parameters of the C67 and C50 functional sheets described in Section 2.6, were directly used as the layer-specific inputs. Each CNT/PET functional sheet and PET interlayer was treated as an equivalent homogeneous transmission-line layer with a thickness of approximately 0.2 mm.

The characteristic impedance and propagation constant of the *i*th layer were calculated as

$$Z_i = Z_0 \sqrt{\frac{\mu_{r,i}}{\varepsilon_{r,i}}}$$

and

$$\gamma_i = j\frac{2\pi f}{c}\sqrt{\mu_{r,i}\varepsilon_{r,i}}$$

respectively, where Z_0 is the impedance of free space, f is the frequency, c is the velocity of light in vacuum, and $\varepsilon_{r,i}$, $\mu_{r,i}$, and d_i are the complex relative permittivity, complex relative permeability, and thickness of the *i*th layer, respectively.

The metal backing was treated as a short-circuit termination:

$$Z_{in,N+1} = 0$$

Starting from the layer adjacent to the metal backing, the input impedance was recursively calculated toward the incident surface according to

$$Z_{in,i} = Z_i \frac{Z_{in,i+1} + Z_i \tanh(\gamma_i d_i)}{Z_i + Z_{in,i+1} \tanh(\gamma_i d_i)}$$

The normalized input impedance magnitude at the air–absorber interface was then obtained as

$$Z_n = \left|\frac{Z_{\text{in},1}}{Z_0}\right|$$

A value of Z_n approaching unity indicates a more favorable overall input-impedance condition for electromagnetic-wave entry. The actual layer sequence adopted for the three P_5-R_{15} structures was

Air → (PET×5→C)×15 → metal backing

where C represents the C100, C67, or C50 functional sheet. The complete structure therefore contained 75 PET interlayers and 15 CNT/PET functional sheets, corresponding to a total thickness of approximately 18.0 mm.

To correlate the calculated input impedance with CNT coverage, the frequency-averaged normalized input impedance magnitude over 2–18 GHz was calculated as

$$\overline{Z}_n = \frac{1}{N_f}\sum_{k=1}^{N_f}\left|\frac{Z_{\text{in}}(f_k)}{Z_0}\right|$$

where N_f is the number of frequency points. The frequency-averaged attenuation constants shown in Fig. S9(c) were obtained by averaging the corresponding attenuation constants of C100, C67, and C50 over the same frequency range.

Because the laterally patterned C67 and C50 functional sheets were represented using an equivalent homogeneous-medium approximation, the calculated input impedance was used to compare the relative coverage-dependent trends of the regularly stacked P_5-R_{15} structures.

Table S1 Microwave absorption performances of representative carbon-based materials

Sample	Thickness /mm	EAB /GHz	Regions of EAB/GHz	Usage of absorbents/(mg·cm^{-3})	Specific usage /(mg·cm^{-3}·GHz^{-1})	Ref.
rGO foam	18	15.6	2.4–18	5.5	0.353	[46]
Carbon nano fiber/CNT	1.7	5.5	10.5–13.2	14	2.55	[47]
CuS@rGO aerogels	2.8	8.44	9.56–18	16	1.89	[48]
Melamine sponge /rGO foam	3.0	7.9	10.82–18	10.7	1.4	[49]
CNT film	2	4.4	12.32–16.72	24.6	5.5	[50]
$NiCo_2O_4$@CNTs sponges	2.5	2.7	7.8–10.5	31.5	11.7	[51]
Porous carbon foams	2.13	7.12	10.88–18	43	6.04	[52]
S67-P_5-R_{15}	18	16	2–18	2.08	0.13	This work